AIAA JOURNAL
Vol. 39, No. 8, August 2001

Fault Identification Using Pseudomodal Energies and Modal Properties

Tshilidzi Marwala*
University of Cambridge, Cambridge, England CB2 1PZ, United Kingdom

The pseudomodal energy, defined as the integrals of the real and imaginary components of the frequency-response functions over various frequency ranges, is proposed for fault identification in structures. Equations that formulate pseudomodal energies in the modal domain and their respective sensitivities are derived in receptance and inertance form. When tested on a simulated cantilevered beam, pseudomodal energies are found to be more resistant to noise in the data than the mode shapes and are able to take into account the out-of-frequency-band modes and to be better indicators of faults than the modal properties. Furthermore, they are more sensitive to faults than the natural frequencies and are equally as sensitive to faults as the mode shapes. The pseudomodal energies are computationally faster to calculate than the modal properties. When tested on a population of 20 steel cylinders, the pseudomodal energies are, on average, better indicators of faults than the modal properties.

Nomenclature

a_q	=	lower frequency bound for the qth pseudomodal energy
b_q	=	upper frequency bound for the qth pseudomodal energy
$[C]$	=	damping matrix
$\{F\}$	=	force input vector
g_p	=	changes in the pth structural parameter
H_{kl}	=	frequency-response function due to excitation at k and measurement at l
j	=	$\sqrt{-1}$
$[K]$	=	stiffness matrix
$[M]$	=	mass matrix
X, X', X''	=	displacement, velocity, and acceleration
$\bar{x}$	=	mean of data
$\{0\}$	=	null vector
ζ_i	=	ith damping ratio
σ	=	standard deviation
$\{\phi\}_i$, $\{\bar{\phi}\}_i$	=	ith mode shape and complex mode shape vector
ω, ω_i, $\bar{\omega}_i$	=	frequency, ith natural frequency, and ith complex natural frequency

Subscripts

i, j, k, l, p, q	=	indices
T	=	transpose

Superscript

N	=	number of measured degrees of freedom or modes

I. Introduction

VIBRATION data have been employed with varying degrees of success to identify damage in structures.[1,2] In this paper, a parameter called pseudomodal energy, which is defined as the integral of the frequency-response function (FRF) over various frequency bandwidths, is introduced for fault identification in structures. In this paper, it is demonstrated that making a thorough study of this parameter offers some insight into how potentially effective this parameter could be of use for fault identification in structures. The analytical expressions defining the pseudomodal energies in receptance and inertance forms are calculated as functions of the modal properties for the case where damping is low. The expressions describing the sensitivities of the pseudomodal energies with respect to any structural modification are derived. The application of the pseudomodal energies for damage identification is studied by comparing the sensitivities of these parameters to those of modal properties.

Monte Carlo simulation[3] is applied to a simulated cantilevered beam (by randomly varying the cross-sectional areas at various positions in the beam) to compare the pseudomodal energies to the modal properties. When such a comparison is made, the sensitivities of these parameters to noise and faults are investigated. The issues on how to choose frequency bandwidths for calculating the pseudomodal energies are discussed in qualitative terms and suggestions on how to optimize the choice of these bandwidths are addressed. Faults are introduced to the cantilevered beam by reducing the cross-sectional area of one of the elements of the beam.

Vibration data from a population of 20 seam-welded cylindrical shells made of steel are measured by exciting the cylinders at various locations using an impulse hammer and measuring vibration responses using an accelerometer located at a fixed position. Each cylinder is divided into three equal substructures, and holes of 10–15 mm are introduced near the centers of each substructure. The modal properties and pseudomodal energies between the undamaged and damaged populations are compared.

II. Modal Properties

Before the pseudomodal energy is introduced, the modal properties, which have been used extensively in fault identification in mechanical systems, are reviewed.[1] Any elastic structure may be expressed in terms of mass, damping, and stiffness matrices in the time domain by the following expression:

$$[M]\{X''\} + [C]\{X'\} + [K]\{X\} = \{F\} \tag{1}$$

If Eq. (1) is transformed into the modal domain to form an eigenvalue equation for the ith mode, then[4]

$$\left(\bar{\omega}_i^2[M] + j\overline{\omega_i}[C] + [K]\right)\{\bar{\phi}\}_i = \{0\} \tag{2}$$

Fox and Kapoor[5] derived the sensitivities of the modal properties (for undamped case) to be

$$\omega_{i,p} = (1/2\omega_i)\left[\{\phi\}_i^T\left[[K]_{,p} - \omega_i^2[M]_{,p}\right]\{\phi\}_i\right] \tag{3}$$

$$\{\phi\}_{i,p} = \sum_{r=1;r\neq i}^{N} \frac{\{\phi\}_r\{\phi\}_r^T}{\omega_i^2 - \omega_r^2}\left[[K]_{,p} - \omega_i^2[M]_{,p}\right]\{\phi\}_i - \frac{1}{2}\{\phi\}_i\{\phi\}_i^T[M]_{,p}\{\phi\}_i \tag{4}$$

Received 7 August 2000; revision received 20 February 2001; accepted for publication 26 February 2001.

*Bradlow Foundation Research Scholar; currently Postdoctoral Research Associate, Department of Electrical and Electronics Engineering, Imperial College, Exhibition Road, London, England SW7 2BT, United Kingdom.

In Eqs. (3) and (4), $\omega_{i,p} = \partial\{\omega\}_i/\partial g_p$, $\{\phi\}_{i,p} = \partial\{\phi\}_i/\partial g_p$, $[K]_{,p} = \partial[K]/\partial g_p$, $[M]_{,p} = \partial[M]/\partial g_p$, and g_p represents changes in the pth structural parameters.

The introduction of damage in structures changes the mass and stiffness matrices. Equations (3) and (4) show that changes in the mass and stiffness matrices cause changes in the modal properties of the structure. Now that the modal properties and their respective sensitivities have been reviewed the next section introduces the pseudomodal energies and their respective sensitivities.

III. Pseudomodal Energies

The pseudomodal energies are defined as the integrals of the real and imaginary components of the FRFs over various frequency ranges that bracket the natural frequencies. The FRFs may be expressed in receptance and inertance form.[4] Receptance expression of the FRF is defined as the ratio of the Fourier-transformed displacement to the Fourier-transformed force. The inertance expression of the FRF is defined as the ratio of the Fourier-transformed acceleration to the Fourier-transformed force. This section expresses pseudomodal energies in terms of receptance and inertance forms in the same way as the FRFs are expressed in these forms. The detailed derivations of equations defining the pseudomodal energies and their derivatives are shown in the Appendix.

A. Receptance and Inertance Pseudomodal Energies

The FRFs may be expressed in terms of the modal properties by using the modal summation equation.[4] From the FRFs expressed as a function of the modal properties, the pseudomodal energies may be calculated as a function of the modal properties. The reason for calculating the pseudomodal energies as a function of the modal properties is so that the capabilities of the pseudomodal energies to identify faults could be inferred from those of the modal properties. The receptance pseudomodal energy (RME) is calculated by integrating the receptance FRF expressed as functions of the modal properties by using the modal summation equation[4] as follows:

$$\mathrm{RME}_{kl}^{q} = \int_{a_q}^{b_q} \sum_{i=1}^{N} \frac{\phi_k^i \phi_l^i}{-\omega^2 + 2\zeta_i \omega_i \omega j + \omega_i^2}\, \mathrm{d}\omega \tag{5}$$

In Eq. (5), a_q and b_q are the lower and the upper frequency bounds, respectively, for the qth pseudomodal energy calculated from the FRF due to excitation at k and measurement at l, and ζ is the damping ratio. The lower and upper frequency bounds bracket the qth natural frequency. When light damping ($\zeta_j \ll 1$) is assumed, Eq. (5) is solved as shown in the Appendix to give[6]

$$\mathrm{RME}_{kl}^{q} = \sum_{i=l}^{N} \frac{\phi_k^i \phi_l^i j}{\omega_i} \left[\arctan\left(\frac{-\zeta_i \omega_i - j b_q}{\omega_i} \right) - \arctan\left(\frac{-\zeta_i \omega_i - j a_q}{\omega_i} \right) \right] \tag{6}$$

The most commonly used techniques to measure vibration data measure the acceleration response instead of the displacement response. In such cases, it is better to calculate the inertance pseudomodal energies (IMEs) as opposed to the RMEs calculated in Eq. (6).

The IME is derived by integrating the inertance FRF written in terms of the modal properties by using the modal summation equation as follows:

$$\mathrm{IME}_{kl}^{q} = \int_{a_q}^{b_q} \sum_{i=l}^{N} \frac{-\omega^2 \phi_k^i \phi_l^i}{-\omega^2 + 2\zeta_i \omega_i \omega j + \omega_i^2}\, \mathrm{d}\omega \tag{7}$$

When it is assumed that damping is low, Eq. (7), as demonstrated in the Appendix, becomes[6]

$$\mathrm{IME}_{kl}^{q} \approx \sum_{i=l}^{N} \left\{ \phi_k^i \phi_l^i (b_q - a_q) - \omega_i \phi_k^i \phi_l^i j \left[\arctan\left(\frac{-\zeta_i \omega_i - j b_q}{\omega_i} \right) - \arctan\left(\frac{-\zeta_i \omega_i - j a_q}{\omega_i} \right) \right] \right\} \tag{8}$$

Equation (8) shows that the IME may be expressed as a function of the modal properties. The IMEs may be calculated directly from the FRFs using any numerical integration scheme without having to go through the process of modal extraction and using Eq. (8). The advantages of using the IMEs as opposed to using the identified modal properties are 1) all of the modes in the structure are taken into account as opposed to using the modal properties, which are limited by the number of modes identified, and 2) integrating the FRFs to obtain the pseudomodal energies smoothes out the zero-mean noise present in the FRFs.

In this section the pseudomodal energies have been mathematically derived (see the Appendix). The next step is to calculate their sensitivities to structural changes the same way Fox and Kapoor[5] calculated the sensitivities of the modal properties with respect to parameter changes.

B. Sensitivities of Pseudomodal Energies

In this section, the sensitivity of pseudomodal energies to parameter changes is assessed. This gives some insights into how these parameters would be affected by the presence of faults in structures. Because the pseudomodal energies have been derived as functions of the modal properties, these sensitivities will also be calculated as functions of the sensitivities of modal properties. The sensitivity of the RMEs are determined by calculating the derivative of Eq. (6) with respect to the pth structural change to give the following expression:

$$\mathrm{RME}_{kl,p}^{q} \approx \sum_{i=l}^{N} \left\{ \begin{array}{l} \left[\dfrac{j}{\omega_i} \left(\phi_{k,p}^i \phi_l^i + \phi_k^i \phi_{1,p}^i \right) - \dfrac{1}{\omega_i^2} j \phi_k^i \phi_l^i \omega_{i,p} \right] \left[\arctan\left(\dfrac{-\zeta_i \omega_i - j b_q}{\omega_i} \right) - \arctan\left(\dfrac{-\zeta_i \omega_i - j a_q}{\omega_i} \right) \right] \\ + \left(\dfrac{j \phi_k^i \phi_1^i}{\omega_i} \right) \left[\dfrac{j b_q \omega_{i,p}}{\omega_i^2 + (\zeta_i \omega_i + j b_q)^2} - \dfrac{j a_q \omega_{i,p}}{\omega_i^2 + (\zeta_i \omega_i + j a_q)^2} \right] \end{array} \right\} \tag{9}$$

Equation (9) is obtained by assuming that $\partial\zeta_q/\partial g_q = 0$ and that $\zeta_q^2 \approx 0$. In this study, faults are introduced by reducing the cross-sectional area of the beam and by drilling holes in structures. Introducing faults this way has been found not to change the damping properties of the structure, thereby justifying the assumption that damping was independent of faults, which is used to derive Eq. (9). Equation (9) shows that the sensitivity of the RME is a function of the natural frequencies, the damping ratios, the mode shapes, and the derivatives of the natural frequencies and mode shapes. Substituting Eqs. (3) and (4) into Eq. (9) gives the sensitivity of the pseudomodal energies in terms of the mass and stiffness matrices, which are directly related to the physical properties of the structure.

The derivative of the IME [Eq. (8)] with respect to the pth parameter changes may be written as follows, as derived in the Appendix:

$$\mathrm{IME}^{q}_{k1,p} \approx \sum_{i=l}^{N} \left\{ \begin{array}{l} (b_q - a_q)\left(\phi^i_{k,p}\phi^i_l + \phi^i_k\phi^i_{l,p}\right) - j\omega_{i,p}\phi^i_k\phi^i_l\left[\arctan\left(\dfrac{-\zeta_i\omega_i - jb_q}{\omega_i}\right) - \arctan\left(\dfrac{-\zeta_i\omega_i - ja_q}{\omega_i}\right)\right] \\ -j\omega_i\left(\phi^i_{k,p}\phi^i_l + \phi^i_k\phi^i_{l,p}\right)\left[\arctan\left(\dfrac{-\zeta_i\omega_i - jb_q}{\omega_i}\right) - \arctan\left(\dfrac{-\zeta_i\omega_i - ja_q}{\omega_i}\right)\right] \\ -j\omega_i\phi^i_{k,p}\phi^i_l\left(\dfrac{jb_q\omega_{i,p}}{\omega_i^2 + 2\zeta_i\omega_i b_q j - b_q^2} - \dfrac{ja_q\omega_{i,p}}{\omega_i^2 + 2\zeta_i\omega_i a_q j - a_q^2}\right) \end{array} \right\} \tag{10}$$

Equations (9) and (10) have been derived in the Appendix. Similarly, Eq. (10) may be expressed in terms of the mass and stiffness matrices by substituting Eqs. (3) and (4) into Eq. (10).

In this section, the RMEs and IME have been derived (see the Appendix), and their respective sensitivities have been calculated. It is shown how these parameters are related to the modal properties, mass, and stiffness matrices. The sensitivities of the RMEs and IMEs are found to depend on the sensitivities of the modal properties. From here onward pseudomodal energy will be used mainly to describe the IME.

When Eqs. (6) and (8) are analyzed, it is observed that, if the frequency bandwidth is too narrow, the pseudomodal energies are dominated by the behavior of the peaks of the FRFs. This is undesirable because, near the peaks, factors such as damping ratios, which show high degrees of uncertainty, dominate the dynamics of the pseudomodal energies. If the bandwidth is too wide, the influence of the antiresonances, which are sensitive to noise, dominates. The optimal way is to choose the bandwidth that is sufficiently narrow to capture the characteristics of the peaks but adequately wide (not to the extent of including the antiresonances) to smooth out the zero-mean noise in the FRFs.

Equations (6) and (8–10) show that the pseudomodal energies depend on the modal properties and the frequency bounds. This implies that as long as the FRF information contains the modal properties, then it does not matter how many frequency points are included in the calculation of the pseudomodal energies. Note that the number of frequency points is a separate issue from the frequency bandwidth. On calculating the pseudomodal energies, the smallest number of frequency points must be used, and this minimizes the errors in the FRFs that are propagated into the pseudomodal energies. In other words, for a given frequency bandwidth for calculating the pseudomodal energies, increasing the number of frequency points in the bandwidth beyond a certain threshold does not necessarily add any additional information about the dynamics of the system. Note that the dynamics of the system is the source of information that indicate the presence or the absence of faults.

Now that expressions for the pseudomodal energies and their respective sensitivities have been derived, as shown in the Appendix, the next objective is to verify these equations. This is done by comparing their sensitivities with respect to the presence of faults in structures calculated directly from the FRFs to those calculated from the modal properties.

IV. Example 1: Cantilevered Beam

A simulated aluminum beam, which is studied in this section, is shown in Fig. 1. A finite element model with nine Euler-beam elements is obtained by using the Structural Dynamics Toolbox,[7] which runs in MATLAB®.[8] The first five natural frequencies were calculated using a finite element model and are 31.4, 197.1, 551.8, 1081.4, and 1787.6 Hz. The FRFs were calculated from the finite element model, then transformed into the time domain, where the data were contaminated with noise, then transformed back to the frequency domain, and then the modal properties were extracted. The FRFs were calculated from the finite element model by following this procedure:

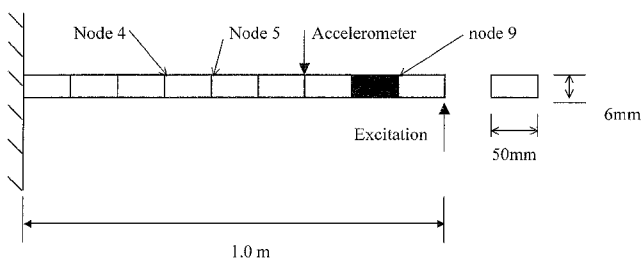

Fig. 1 Cantilevered beam modeled with nine Euler beam elements.

1) Use the finite element model to calculate the first 18 modal properties.

2) Assume the damping ratios of 0.001, and use the modal summation equation[4] to generate the FRFs of frequency bandwidth [0.8545 7000] Hz. (The size of the FRFs is 8192.)

3) Generate the mirror image of the FRFs centered on 0 Hz. (New frequency bandwidth is [−7000 7000] Hz.)

4) On the FRFs generated in step 3, perform the inverse fast Fourier transform[9] to obtain the impulse response function (of size 16,384).

5) Add uniform noise levels (±0, ±1, ±2, ±3, and ±4%) to the impulse response data.

6) Perform the fast Fourier transform to the impulse response function to obtain the FRFs (of size 8192).

From the FRFs calculated in step 6, the modal properties were extracted as follows:

1) Choose the frequency bandwidth for mode extraction ([17 1880] Hz).

2) Obtain the initial estimates of the natural frequencies and damping ratios. It was assumed that the natural frequencies and damping ratios were known. (The natural frequencies were taken from the finite element model and damping ratios were set to be 0.001.)

3) Use the natural frequencies and damping ratios in step 2 to calculate the mode shapes.

Various fault cases were simulated by reducing the cross-sectional area of element 8 (Fig. 1) by 5, 10, and 15%. For each fault case and the undamaged case, the FRFs were generated. From these FRFs, the modal properties were extracted as described in the preceding paragraph, and the pseudomodal energies were calculated by integrating over the FRFs using the trapezoidal rule technique. When the pseudomodal energies were calculated, the following bandwidths were chosen to bracket the natural frequencies of the beam: 18–44, 155–240, 484–620, 1014–1151, and 1726–1863 Hz.

Monte Carlo simulation with 1000 samples was performed by choosing a fault case and noise level and then varying the cross-sectional area of all nine elements by 1% Gaussian noise. The same procedure was performed when element 8 was reduced by 5, 10, and 15%. In other words, the abilities of the modal properties and pseudomodal energies to detect faults of 5, 10, and 15% reduction in cross-sectional area of element 8 (Fig. 1) were assessed despite the presence of ±1% perturbations in cross-sectional areas of all nine elements.

The sensitivities of the pseudomodal energies and modal properties to damage were investigated in the presence of various noise levels by using the statistical overlap factor (SOF). The SOF between two distributions is defined as the ratio of the distance between the averages of the two distributions to the mean of the two standard deviations. The SOF may be written mathematically as follows:

$$\mathrm{SOF} = \left| \frac{\bar{x}_1 - \bar{x}_2}{(\sigma_1 + \sigma_2)/2} \right| \tag{11}$$

where $\bar{x}_1$ and $\bar{x}_2$ are the means of distributions and σ_1 and σ_2 are their respective standard deviations.

The SOF was inspired by the modal overlap factor, which is widely used in modal analysis to assess the degree of modal overlap

between two modes.[10] The higher the SOF, the better is the degree of separation between the two distributions. The influence of noise on the pseudomodal energies and modal properties, as well as the effect of excluding high-frequency modes when identifying these parameters, was investigated.

V. Example 1: Results and Discussion

A. Confirmation of Equations (8) and (10)

This section verifies the accuracy of Eqs. (8) and (10). To verify the accuracy of Eq. (8), the pseudomodal energies were calculated from this equation (using the modal properties extracted from the FRFs) and from numerical integration of the FRFs. Note that the FRFs used in this section were not contaminated with noise. The results of the real and imaginary parts of the pseudomodal energies are shown in Fig. 2. These graphs show that the real and imaginary parts of the pseudomodal energies from Eq. (8) are close to those from numerical integration. The absolute percentage differences of the real part of pseudomodal energies shown in Fig. 2 is 8% for the first mode, 1% for the second mode, 0% for the third mode, 3% for the fourth mode, and 30% for the fifth mode. The imaginary part shows the absolute percentage differences of 4% for the first mode and 0% for the second–fifth mode. The reason for the inaccuracy on the fifth and the first modes for the real and imaginary parts of the pseudomodal energies, respectively, is because of their relative small magnitudes, making them susceptible to numerical errors.

Likewise, to confirm the accuracy of Eq. (10), the sensitivities of the pseudomodal energies obtained from using Eq. (10) were compared to those from numerical integration of the FRFs, and the results are shown in Fig. 3. Figure 3 shows that the two procedures give similar results of the real and imaginary parts of these sensitivities. The percentage differences between the real part of the sensitivities of the pseudomodal energies are approximately 0% for all modes. For the imaginary part, the difference is approximately 0% for the first three modes as well as 2 and 4% for the fourth and fifth modes. The reason why some modes have higher differences than others is because of the numerical errors encountered when calculating the sensitivities of the pseudomodal energies. In this section, Eqs. (8) and (10) were proven to give results similar to those obtained through direct integration of the FRFs.

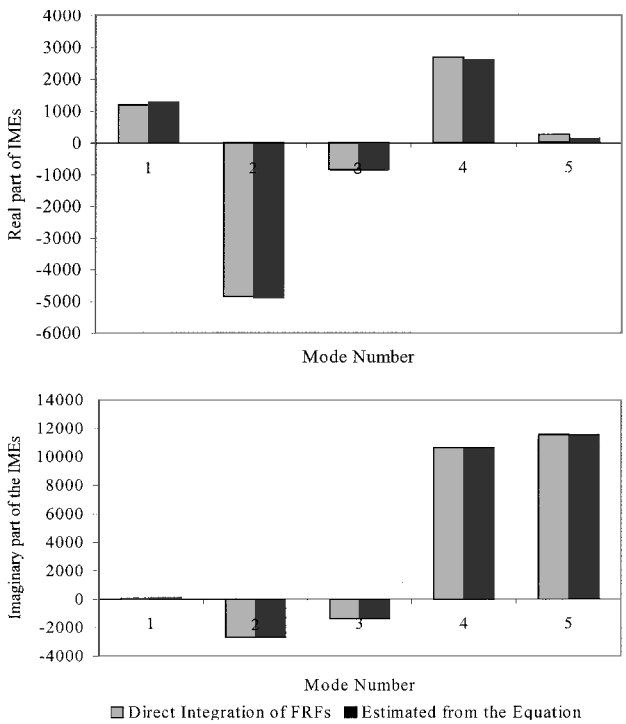

Fig. 2 Real and imaginary parts of the pseudomodal energies obtained using direct integration of the FRF and calculated from the modal properties using Eq. (8). (The FRF is noise free.)

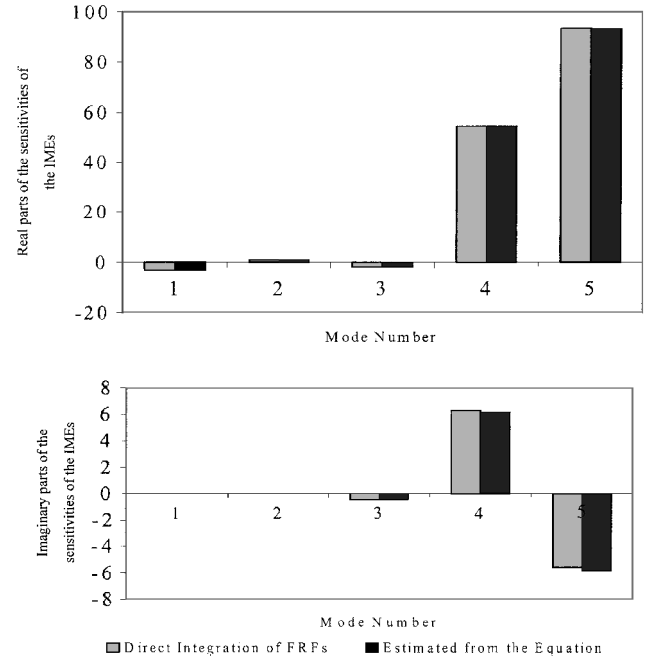

Fig. 3 Real and imaginary parts of the sensitivities of the pseudomodal energies due to 1% reduction in cross-sectional area of element 8, calculated from direct integration of the FRF and from Eq. (10). (The FRF is noise free.)

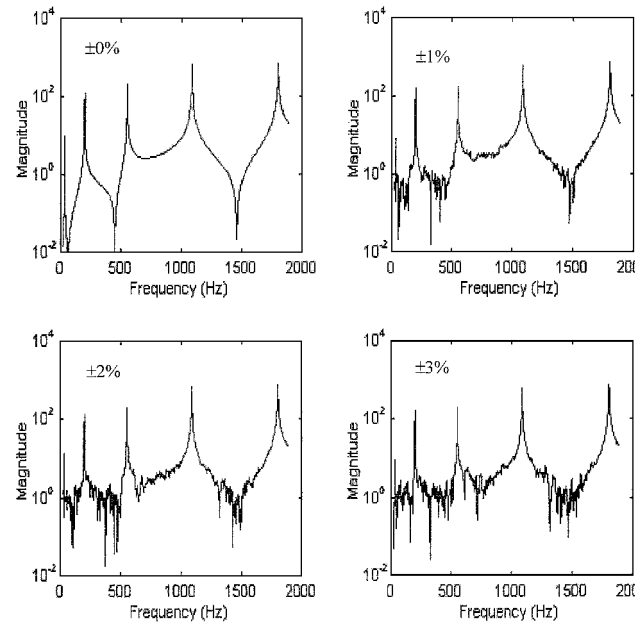

Fig. 4 Magnitudes of the FRFs obtained using the time-domain data contaminated with ± 0, ± 1, ± 2, and ± 3% noise.

B. Influence of Noise on the Pseudomodal Energies and Modal Properties

One issue that is important in fault identification is that the inevitable presence of noise in the data must be such that the effects are less influential than those of faults. It has been observed in the literature[1] that, for some fault types, the changes in the modal properties due to faults are more visible than the variations in measured data due to noise. This makes the modal properties viable data for fault identification. The modal properties and pseudomodal energies before damage were calculated with various noise levels added to the time-domain data. Figure 4 shows the sample FRF with various noise levels added to the time-domain data. Figure 4 shows that the effects of noise on the FRFs are mostly observable in the antiresonances.

The other issue to be resolved was to assess the effect of the presence of noise in the data on the modal properties and pseudomodal

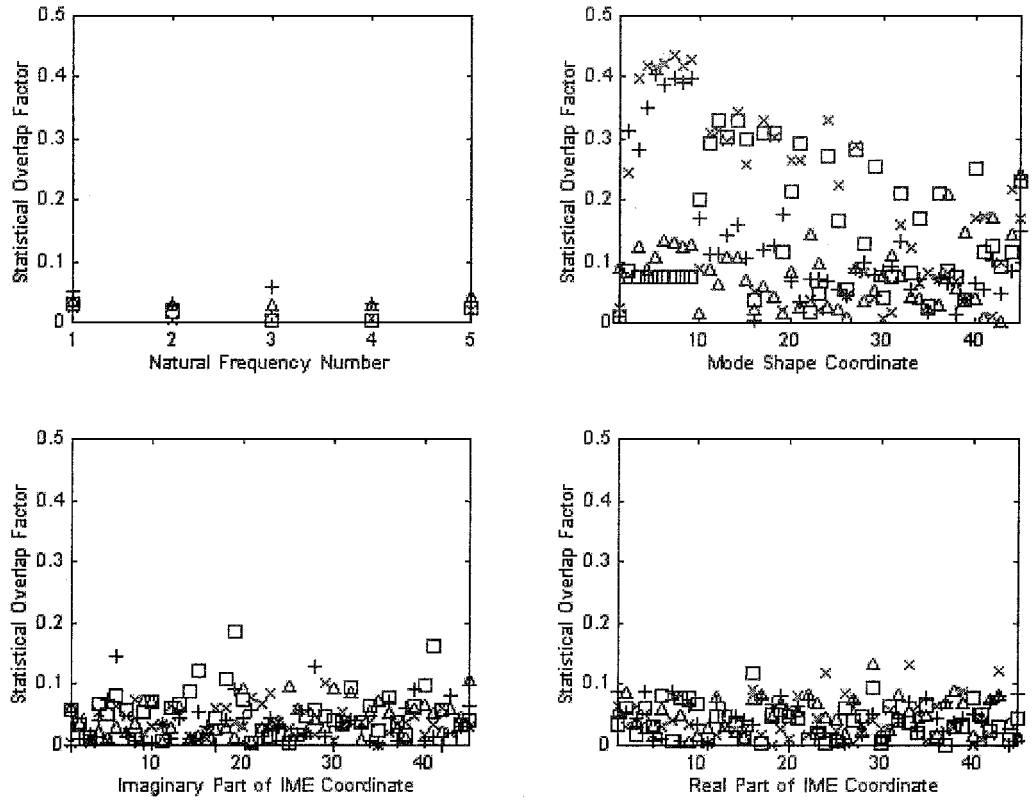

Fig. 5 SOFs for undamaged cases between 0% noise and various noise levels for the natural frequencies, mode shapes, and imaginary and real parts of the pseudomodal energies: △, 1% noise; +, 2% noise; × 3% noise; and □, 4% noise.

energies. To achieve this goal, Monte Carlo simulation was performed by running the finite element model 1000 times and each time introducing noise in the vibration data. From these data, the modal properties and pseudomodal energies were calculated. The noise levels added to the vibration data were 1–4% Gaussian noise.

The SOFs between the distribution of the Monte Carlo simulated data with zero noise added and those from the data simulated with 1–4% noise added are shown in Fig. 5. Figure 5 shows that the pseudomodal energies are, on average, about five times more resistant to noise than the mode shapes. Natural frequencies are found to be the most resistant to noise than the other three parameters. It is noted later that the natural frequencies are not only resistant to noise as demonstrated in Fig. 5 but are also insensitive to faults (Fig. 6). The pseudomodal energies are more resistant to noise than the mode shapes because 1) performing numerical integration on the FRFs to obtain the pseudomodal energies smoothes out the zero-mean noise and 2) the optimization nature of modal analysis introduces additional uncertainties. In addition, modal properties show high susceptibility to noise because of the inclusion of mode 1, which is noisier than other modes (Fig. 4). The issue mentioned in step 2 illustrates the main limitation of modal analysis where the inclusion of a mode with high noise level compromises the identification of other modes.[7]

In this section, the pseudomodal energies were found to be, on average, more resistant to noise than the mode shapes. The natural frequencies are found to be more resistant to noise than the other three parameters. Their resistance to noise on the measured data is one of the essential requirements in fault identification even though it is not a sufficient condition for successful fault identification in structures. The most essential feature is the sensitivity of faults to parameter changes, which is the subject of the next section.

C. Changes in the Pseudomodal Energies and Modal Properties due to Damage

In this section, the pseudomodal energies are compared to the modal properties using data simulated from the cantilevered beam. It was demonstrated in Eq. (10) that the sensitivity of the pseudomodal energies are functions of the sensitivities of the modal properties, implying that these parameters are not necessarily independent. The cross-sectional area of element 8 in Fig. 1 was reduced by 0, 5, 10, and 15%. In the presence of these reductions of cross-sectional area of element 8, Monte Carlo simulation with 1000 samples was performed by perturbing the cross-sectional area of all of the elements by 1% Gaussian noise.

The four distributions of the pseudomodal energies and modal properties from Monte Carlo simulation were used to calculate the SOFs between 0 and 5%, 0 and 10%, as well as 0 and 15% reductions in cross-sectional areas. The results are shown in Fig. 6. Figure 6 shows that the pseudomodal energies and mode shapes show sensitivity to faults. When Fig. 5 is compared to Fig. 6, it is observed that that the pseudomodal energies about equally indicate faults as the mode shapes. However, the pseudomodal energies are more resistant to noise than the mode shapes. The natural frequencies are found to be less sensitive to faults than the other three parameters. Figure 6 also shows that, on average, the more severe the faults are, the higher the SOFs.

The sample distributions of the modal properties and pseudomodal energies used to calculate the SOFs shown in Fig. 6 are shown in Fig. 7. Figure 7 indicates that the reduction in cross-sectional area of element 8 does not change the natural frequencies significantly enough to show separate distributions. Figure 7 shows that the mode shapes, as well as the real and imaginary parts of the IMEs, show four different distributions, which indicates that these fault cases are separable. The distributions of the imaginary part of the IMEs for various fault cases are the most separable followed by that of the real part of the IMEs, then the mode shapes, and finally the natural frequencies.

The mode shapes and pseudomodal energies correspond to mode 4 and coordinate corresponding to node 3. Note that in real measurements natural frequencies are measured to the accuracy of 1 Hz and mode shapes to the accuracy of 10% (Ref. 11). Therefore, the natural frequency shown in Fig. 7 will not be able to diagnose even 15% reduction in cross-sectional area of element 8. However, Fig. 7 is shown to highlight the differences in the distributions between various types of data. This section has demonstrated that the pseudomodal energies are, on average, better indicators of faults

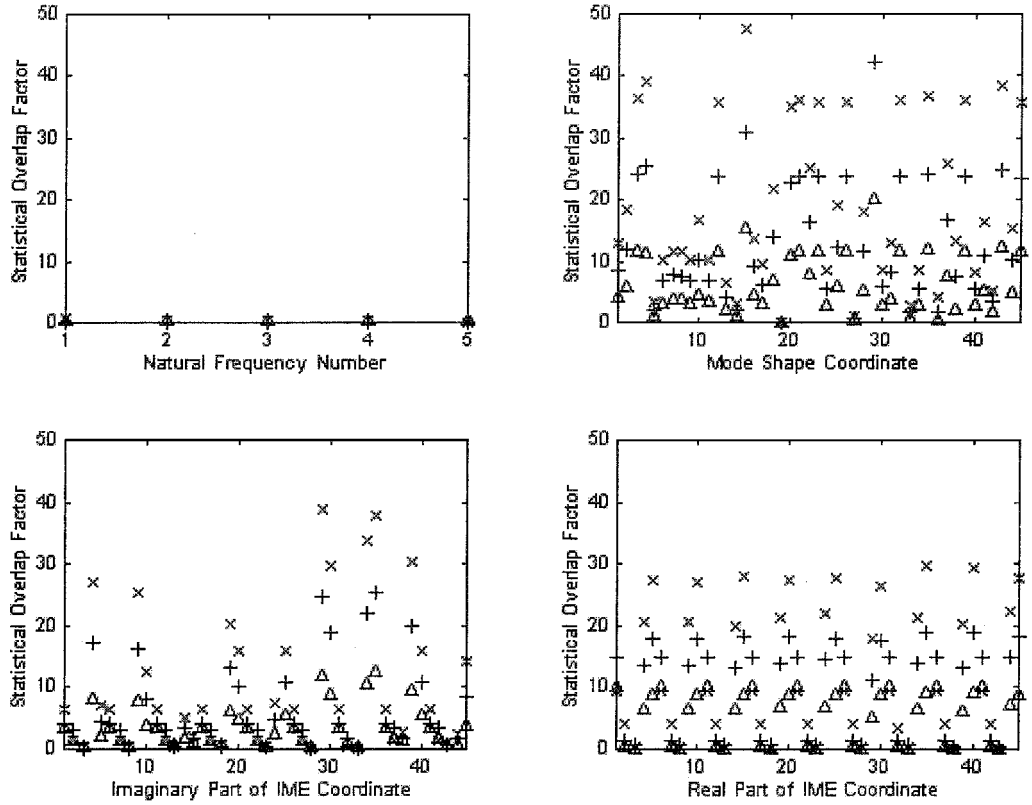

Fig. 6 SOFs between 0% reduction and various reductions (5, 10, and 15%) in cross-sectional area of element 8 for the natural frequencies, mode shapes, and imaginary and real part of the pseudomodal energies due to damage: △, 5% reduction; +, 10% reduction; and ×, 15% reduction.

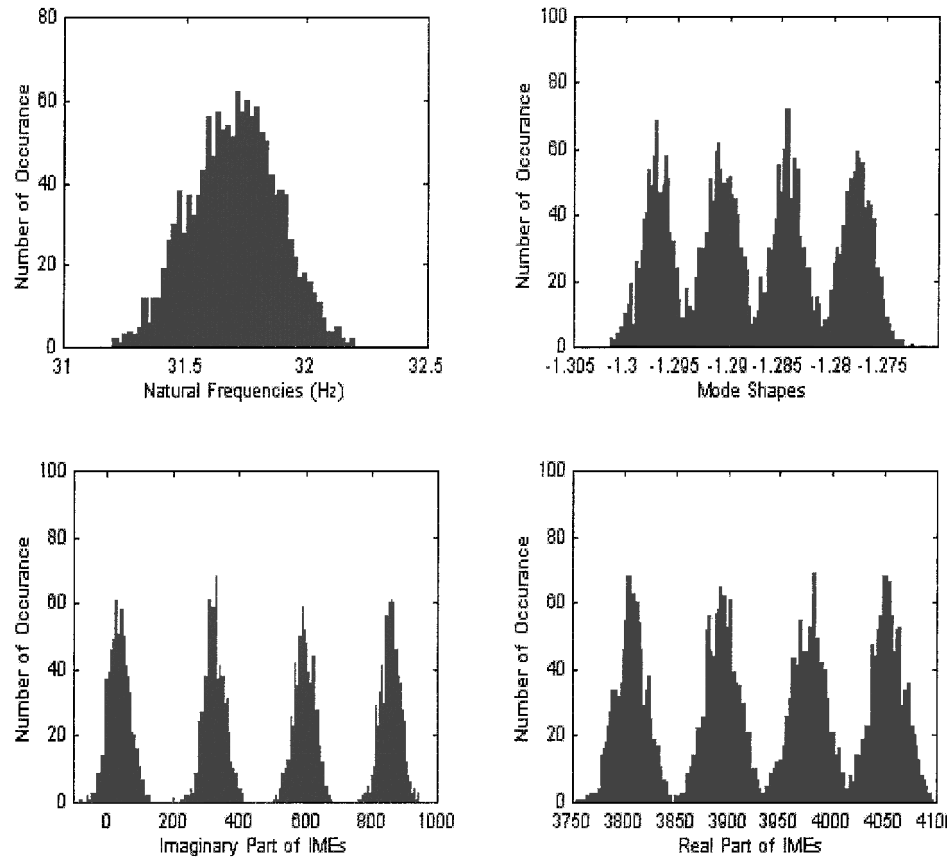

Fig. 7 Distributions of the first natural frequencies, the mode shape coordinate, and the imaginary and real parts of the pseudomodal energies for various reductions in cross-sectional area of element 8.

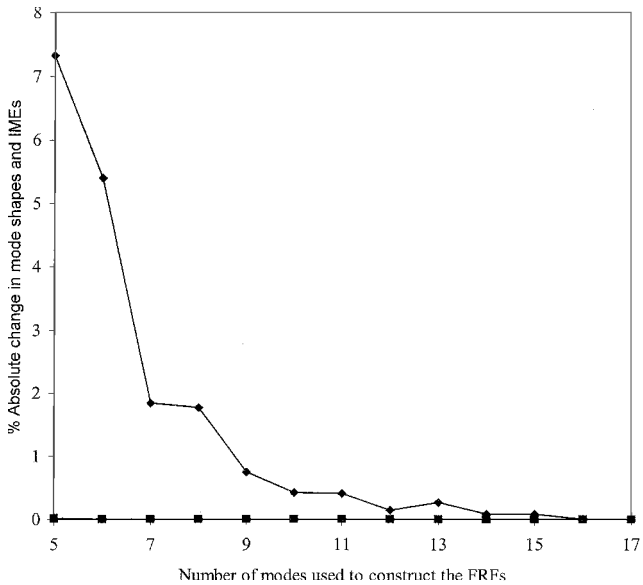

Fig. 8 Percentage differences between the mode shapes and pseudomodal energies identified from the FRFs calculated using the first 5–17 modes and from the first 18 modes: ♦, real part of IMEs; ■, imaginary part of the IMEs; and ■, mode shapes.

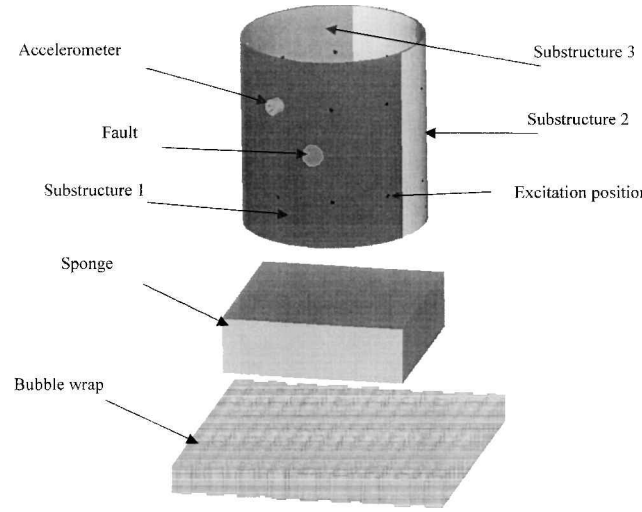

Fig. 9 Cylindrical shell.

than the natural frequencies and are equally as good indicators of faults as the mode shapes.

D. Effects of Excluding High-Frequency Modes

This section will assess the ability of the pseudomodal energies and modal properties to capture the information from the frequencies that lie outside the frequency bandwidth of interest. In this paper, the FRFs were calculated from the modal properties. In physical structures, the FRFs are constructed from all of the excited modes in the structure. For a simulated beam used in this paper, constructing FRFs using 18 modes represents the real structure. Because high modes were required, the finite element model was remeshed so that it contained 50 elements. This was done to improve the accuracy of higher modes. The results showing the effect of excluding high modes on the identification of pseudomodal energies and modal properties are shown in Fig. 8. Figure 8 shows the average absolute percentage difference between data obtained using FRFs that were calculated using the first 18 modes and those obtained using the first 5–17 modes. The natural frequencies are not shown here because they are not sensitive to the inclusion of higher modes. Figure 8 shows that the exclusion of higher modes does not affect the identified mode shapes and imaginary parts of the pseudomodal energies. However, the real parts of the pseudomodal energies are found to be sensitive to the exclusion of high modes.

VI. Example 2: Experimental Procedure

The proposed pseudomodal energies are compared to the modal properties using a population of cylinders, which were supported by inserting a sponge and rested on a bubble wrap, to simulate a free–free environment (Fig. 9). The sponge was inserted inside the cylinders to control boundary conditions. Conventionally, free–free environment is achieved by suspending a structure. In this paper, this is avoided because it is relatively less convenient to suspend the structure (especially a population of structures in an assembly line settings) compared to just resting it on a bubble wrap.

The impulse hammer test was performed on each of the 20 steel seam-welded cylindrical shells (1.75 ± 0.02 mm thickness, 101.86 ± 0.29 mm diam, and 101.50 ± 0.20 mm height). The impulse was applied at 19 different locations, as indicated in Fig. 9, 9 on the upper half of the cylinder and 10 on the lower half of the cylinder. The maximum sampling rate is set to 10 kHz, which is sufficient for the frequency bandwidth of interest, that is 0–5000 Hz. Some of the problems that were encountered during impulse testing included the difficulty of exciting the structure at an exact position (especially for an ensemble of structures) and in a repeatable direction. Each cylinder was divided into three equal substructures (indicated by different shades in Fig. 9), and holes of 10–15 mm were introduced near the centers of the substructures to simulate faults.

For one cylinder, the first type of fault was a zero-fault scenario. This type of fault was given the identity [0 0 0], indicating that there were no faults in any of the substructures. The second type of fault was a one-fault scenario, where a hole may be located in any of the three equal substructures. Three possible one-fault scenarios were [1 0 0], [0 1 0], and [0 0 1] indicating one hole in substructures 1, 2, or 3, respectively. The third type of fault was a two-fault scenario, where one hole was located in two of the three substructures. Three possible two-fault scenarios were [1 1 0], [1 0 1], and [0 1 1]. The final type of fault was a three-fault scenario, where a hole located in all three substructures, and the identity of this fault was [1 1 1]. There were eight different types of fault cases considered (including [0 0 0]).

Because the zero-fault scenarios and the three-fault scenarios were overrepresented, 12 cylinders were picked at random and additional one- and two-fault cases were measured after increasing the magnitude of the holes. This was done before the next fault case was introduced to the cylinders. The reason why only a few fault cases were selected was because of the limited computational storage space available. For each fault case, acceleration and impulse measurements were taken. The types of faults that were introduced, that is, drilled holes, do not influence damping significantly.

Each cylinder was measured three times under different boundary conditions by changing the orientation of a rectangular sponge inserted inside the cylinder. The number of sets of measurements taken for undamaged population is 60 (20 cylinders × 3 for different boundary conditions).

From the measured data, the FRFs are calculated. The frequency spacing of the FRFs is 1.22 Hz. From the FRFs, the modal properties are extracted using the Structural Dynamic Toolbox,[7] and the pseudomodal energies are calculated by using the trapezoidal rule. When the pseudomodal energies were calculated, frequency ranges spanning over 6% of the natural frequencies were chosen. These bandwidths are as follows: 393–418, 418–443, 536–570, 1110–1180, 1183–1254, 1355–1440, 1450–1538, 2146–2280, 2300–2440, 2250–2401, 2500–2656, 3140–3340, 3350–3565, 3800–4039, and 4200–4458 Hz.

A. Modal Properties and Pseudomodal Energies

The modal properties and pseudomodal energies were chosen by employing the following five steps:

1) Find the means and the standard deviations of the modal properties and pseudomodal energies at each index for data from undamaged and damaged cylinders, for example, mode 5 coordinate 3 is assigned its own index number. Here an index is any whole number.

2) Calculate the difference between the means of the data from undamaged and damaged cylinders at each index.

3) Calculate the average of the standard deviations from undamaged and damaged cylinders while keeping track of the indices.

4) Calculate the SOF, defined as the absolute value of the ratio between the average differences in step 2 to the average standard deviations in step 3 at each data index.

5) From the SOFs, select 19 indices with the highest ratios and assess their corresponding data.

B. Results and Discussion

The SOFs between the data from undamaged and damaged cylinders (only a one-fault case) are shown in Fig. 10. Figure 10 shows that the SOFs for the pseudomodal energies are higher than that of the modal properties. This implies that for the pseudomodal energies it easier to separate the distribution of the data from structures with a single hole from that of undamaged structure than for the modal properties.

Figure 11 shows the statistical overlap factors obtained when comparing the modal properties between various fault cases. Figure 11 shows that the first 19 most reliable and sensitive modal properties show the statistical overlap factors varying from 0.0073 to 2.5577 with an average of 0.63. Figure 12 is similar to this but uses the pseudomodal energies, and the SOFs are found to vary from 0.0243 to 2.286 with an average of 0.91. The observation that the average SOF for the pseudomodal energies is higher than that of the modal properties implies that the distributions of the pseudomodal properties for various fault cases are relatively easier to distinguish than those calculated using the modal properties.

The results shown in Figs. 10–12 are summarized in Table 1. Table 1 shows that the pseudomodal energies are able to separate the zero-fault case from the one-fault, two-fault, and three-fault cases better than the modal properties. Furthermore, the pseudomodal energies are able to separate the one-fault case from the two-fault case better than the modal properties. The modal properties are able to separate the two-fault case from the three-fault case better than the pseudomodal energies.

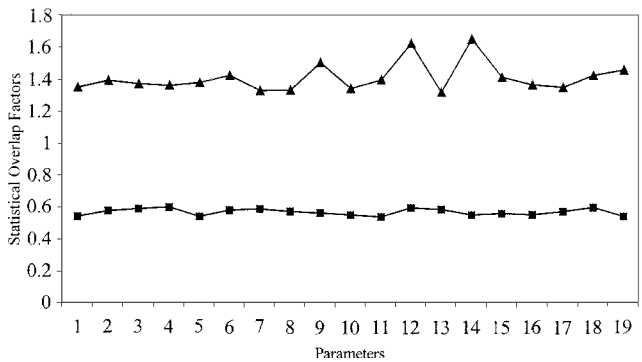

Fig. 10 Graph of SOFs between data from undamaged and damaged cylinders (one-fault case): ▲, modal energy, and ■, modal property.

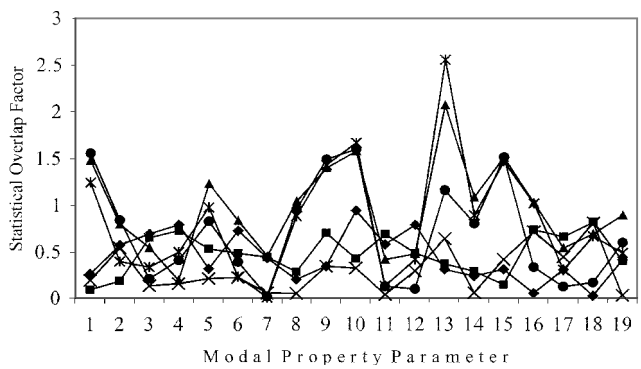

Fig. 11 Graph of SOFs between the modal properties from the undamaged and the damaged cylindrical shells; 0 and 1 (bottom) indicate the SOFs between the distribution of all of the zero-fault and one-fault cases over the entire population of cylinders: ♦, 0 and 1; ■, 0 and 2; ▲, 0 and 3; ×, 1 and 2; ✳, 1 and 3; and ●, 2 and 3.

Table 1 Average statistical overlap factors between various fault cases

Parameter	0 and 1[a]	0 and 2	0 and 3	1 and 2	1 and 3	2 and 3
Modal properties	0.44	0.48	0.96	0.36	0.82	0.70
Pseudomodal energies	1.01	1.54	1.59	0.48	0.62	0.26

[a]SOFs between the distribution of zero-fault and one-fault cases.

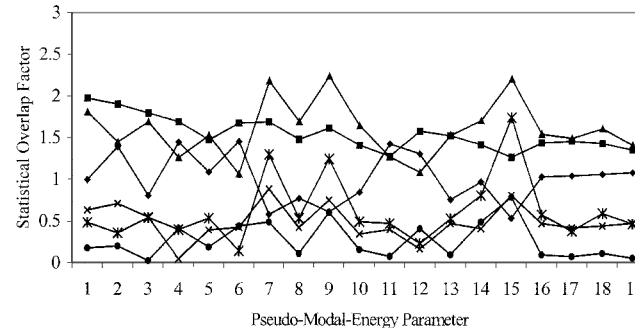

Fig. 12 Graph of SOFs between the pseudomodal energies from the undamaged and the damaged cylindrical shells; 0 and 1 (bottom) indicate the SOFs between the distribution of all of the zero-fault and one-fault cases over the entire population of cylinders: ♦, 0 and 1; ■, 0 and 2; ▲, 0 and 3; ×, 1 and 2; ✳, 1 and 3; and ●, 2 and 3.

VII. Computational Load

The time taken to compute the mode shapes using the Structural Dynamics Toolbox[7] was 3.19 CPU seconds. (This does not include the time taken to obtain the first estimates of the natural frequencies.) On the other hand, the time taken to compute the pseudomodal energies is 0.11 CPU seconds. Monte Carlo simulation with 1000 samples required 270 CPU minutes. All of the computations were performed on a Pentium 200-MHz personal computer with 32 RAM.

VIII. Conclusions

The pseudomodal energies have been proposed and used to detect faults in a simulated cantilevered beam and compared to the modal properties by using SOFs and Monte Carlo simulation. The pseudomodal energies are, on average, found to be equally sensitive to faults as the mode shapes. Furthermore, the pseudomodal energies are found to be more resistant to noise than the mode shapes. Their resistance to noise is attributed to the calculation of the pseudomodal energies by integrating the FRFs directly, which smoothes out the zero-mean noise present in the FRFs. The real parts of the pseudomodal energies are found to take into account the information from high-frequency modes, whereas the modal properties do not. The pseudomodal energies are found to be at least 30 times faster to compute and to be a better alternative to fault identification than the most widely used modal properties. When vibration data from a population of cylinders are used, it has been observed that the pseudomodal energies are, on average, better indicators of faults than the modal properties.

Appendix: Derivation

Expressions for pseudomodal energies are derived in detail in terms of the modal properties. Furthermore, the sensitivities of the pseudomodal energies are expressed in terms of the sensitivities of modal properties of Fox and Kapoor.[5] In vibration analysis, mechanical structures can be excited using the modal hammer and vibration response measured. If the discrete Fourier transform is applied to the displacement response $X(t)$ and the excitation $F(t)$, then $X(\omega)$ and $F(\omega)$, respectively,[4] are obtained. The $X(\omega)$ and $F(\omega)$ are the displacement and force histories in the frequency domain. The receptance FRF $H_{kl}(\omega)$ due to the excitation at k and measurement at l is defined as the ratio of the transformed displacement response $X(\omega)$ to the transformed excitation $F(\omega)$ by

$$H_{kl}(\omega_i) = \frac{X_l(\omega_i)}{F_k(\omega_i)} \tag{A1}$$

The receptance FRF in Eq. (A1) is related to the mass and stiffness matrices by[4]

$$[H(\omega)] = [-\omega^2[M] + j\omega[C] + [K]]^{-1} \tag{A2}$$

The inertance FRF is defined as

$$\ddot{H}_{kl}(\omega_i) = \frac{-\omega_i^2 X_l(\omega_i)}{F_k(\omega_i)} \tag{A3}$$

The receptance FRF in Eq. (A1) may be written in terms of the modal properties (natural frequencies, damping ratios, and mode shapes) by using the modal summation equation[4] by assuming that damping is low as follows:

$$H_{kl}(\omega) = \sum_{i=l}^{N} \frac{\phi_k^i \phi_l^i}{-\omega^2 + 2\zeta_i\omega_i\omega j + \omega_i^2} \tag{A4}$$

where the contribution of each mode is given by the natural frequency ω_i and damping ratio ζ_i and ϕ_k^i is the kth entry of the ith normalized mode shape vector. These FRFs are transformed into the pseudomodal energies defined as the integrals of the real and imaginary components of the FRFs over various frequency ranges. The RMEs are calculated as follows[6]:

$$\begin{aligned}
\mathrm{RME}_{kl}^q &= \int_{a_q}^{b_q} \sum_{i=l}^{N} \frac{\phi_k^i \phi_l^i}{-\omega^2 + 2\zeta_i\omega_i\omega j + \omega_i^2}\,\mathrm{d}\omega \\
&= \left| \sum_{i=l}^{N} \frac{2\phi_k^i \phi_l^i j}{\sqrt{4\omega_i^2 - 4\zeta_i^2\omega_i^2}} \left[\arctan\left(\frac{-\zeta_i\omega_i - j\omega}{\omega_i\sqrt{1-\zeta_i^2}} \right) \right] \right|_{a_q}^{b_q} \\
&= \sum_{i=l}^{N} \frac{\phi_k^i \phi_l^i j}{\omega_i\sqrt{1-\zeta_i^2}} \left[\arctan\left(\frac{-\zeta_i\omega_i - jb_q}{\omega_i\sqrt{1-\zeta_i^2}} \right) \right. \\
&\quad \left. - \arctan\left(\frac{-\zeta_i\omega_i - ja_q}{\omega_i\sqrt{1-\zeta_i^2}} \right) \right]
\end{aligned} \tag{A5}$$

The sensitivity of the RME in Eq. (A6) with respect to any parameter changes may be written in the following form:

$$\mathrm{RME}_{kl,p}^q = \sum_{i=l}^{N} \left[\left(\frac{j\phi_k^i \phi_l^i}{\omega_i} \right)_{i,p} B_{kl}^q + \left(\frac{j\phi_k^i \phi_l^i}{\omega_i} B_{kl,p}^q \right) \right] \tag{A7}$$

The results in Eq. (A7) assume that $\partial\zeta_i/\partial g_p = 0$ and the term $B_{kl,p}^q$ stands for $\partial B_{kl,p}^q/\partial g_i$, where

$$B_{kl}^q = \arctan[(-\zeta_i\omega_i - jb_q)/\omega_i] - \arctan[(-\zeta_i\omega_i - ja_q)/\omega_i] \tag{A8}$$

The derivative $B_{kl,p}^q$ is calculated to be

$$\begin{aligned}
B_{kl,p}^q &= \frac{1}{1 + [(-\zeta_i\omega_i - jb_q)/\omega_i]^2} \\
&\quad \times \left[\frac{-\zeta_i\omega_i\omega_{i,p} - (-\zeta_i\omega_i - jb_q)\omega_{i,p}}{\omega_i^2} \right] \\
&\quad - \frac{1}{1 + [(-\zeta_i\omega_i - ja_q)/\omega_i]^2} \\
&\quad \times \left[\frac{-\zeta_i\omega_i\omega_{i,p} - (-\zeta_i\omega_i - ja_q)\omega_{i,p}}{\omega_i^2} \right] \\
&= \frac{jb_q\omega_{i,p}}{\omega_i^2 + (\zeta_i\omega_i + jb_q)^2} - \frac{ja_q\omega_{i,p}}{\omega_i^2 + (\zeta_i\omega_i + ja_q)^2}
\end{aligned} \tag{A9}$$

$$\begin{aligned}
\left(j\phi_k^i\phi_l^i/\omega_i\right)_{,p} &= \left[j\omega_i\left(\phi_k^i\phi_l^i\right)_{,p} - j\phi_k^i\phi_l^i\omega_{i,p}\right]/\omega_i^2 \\
&= (j/\omega_i)\left(\phi_{k,p}^i\phi_l^i + \phi_k^i\phi_{1,p}^i\right) - \left(1/\omega_i^2\right)j\phi_k^i\phi_l^i\omega_{i,p}
\end{aligned} \tag{A10}$$

When Eqs. (A8–A10) are substituted into Eq. (A7), the derivatives of the RMEs with respect to parameter changes may be written as follows:

$$\begin{aligned}
\mathrm{RME}_{kl,p}^q = \sum_{i=l}^{N} \left\{ \right. & \left[\frac{j}{\omega_i}\left(\phi_{k,p}^i\phi_l^i + \phi_k^i\phi_{l,p}^i\right) - \frac{j}{\omega_i^2}j\phi_k^i\phi_l^i\omega_{i,p} \right] \left[\arctan\left(\frac{-\zeta_i\omega_i - jb_q}{\omega_i} \right) - \arctan\left(\frac{-\zeta_i\omega_i - ja_q}{\omega_i} \right) \right] \\
& \left. + \left(\frac{j\phi_k^i\phi_l^i}{\omega_i} \right) \left[\frac{jb_q\omega_{i,p}}{\omega_i^2 + (\zeta_i\omega_i + jb_q)^2} - \frac{ja_q\omega_{i,p}}{\omega_i^2 + (\zeta_i\omega_i + ja_q)^2} \right] \right\}
\end{aligned} \tag{A11}$$

In Eqs. (A5), a_q and b_q are the lower and the upper frequency bounds for the qth pseudomodal energy calculated from the FRF due to the excitation at k and measurement at l. The advantage of this equation is that the pseudomodal energies may be calculated directly using any numerical integration scheme without having to go through the process of modal extraction. When light damping ($\zeta_j \ll 1$) is assumed, Eq. (A5) becomes

$$\begin{aligned}
\mathrm{RME}_{kl}^q &\approx \sum_{i=l}^{N} \frac{\phi_k^i \phi_l^i j}{\omega_i} \left[\arctan\left(\frac{-\zeta_i\omega_i - jb_q}{\omega_i} \right) \right. \\
&\quad \left. - \arctan\left(\frac{-\zeta_i\omega_i - ja_q}{\omega_i} \right) \right]
\end{aligned} \tag{A6}$$

Equation (A11) shows that the sensitivity of pseudomodal energies is a function of the natural frequencies and mode shapes and their respective derivatives. When the derivatives of the mass, damping, and stiffness matrices using expressions given by Fox and Kapoor[5] are substituted, Eq. (A11) gives the sensitivity of the RMEs in terms of the mass and stiffness matrices, which are directly related to the physical properties. This shows that the pseudomodal energies may be related directly to the physical properties of the structure.

Some of the techniques that are used to measure the vibration data measure the acceleration instead of the displacement. In such a case, it is relatively more efficient to calculate the IMEs.[6] The IMEs are derived as follows:

$$\begin{aligned}
\mathrm{IME}_{kl}^q &= \int_{a_q}^{b_q} \sum_{i=l}^{N} \frac{-\omega^2\phi_k^i\phi_l^i}{-\omega^2 + 2\zeta_i\omega_i\omega j + \omega_i^2}\,\mathrm{d}\omega = \left| \sum_{i=l}^{N} \phi_k^i\phi_l^i\omega + \phi_k^i\phi_l^i\zeta_i\omega_i j\ln\left(-\omega^2 + 2\zeta_i\omega j + \omega_i^2\right) + \left(2\zeta_i^2\omega_i^2 - \omega_i^2\right) \int \frac{\phi_k^i\phi_l^i\,\mathrm{d}\omega}{-\omega^2 + 2\zeta_i\omega_i\omega j + \omega_i^2} \right|_{a_q}^{b_q} \\
&= \sum_{i=l}^{N} \left\{ \begin{array}{l} \phi_k^i\phi_l^i(b_q - a_q) + \zeta_i\omega_i\phi_k^i\phi_l^i j \left[\ln\left(\dfrac{-b_q^2 + 2\zeta_i\omega_i b_q j + \omega_i^2}{-a_q^2 + 2\zeta_i\omega_i a_q j + \omega_i^2} \right) \right] \\ + \left(2\zeta_i^2\omega_i^2 - \omega_i^2\right) \dfrac{\phi_k^i\phi_l^i j}{\omega_i} \left[\arctan\left(\dfrac{-\zeta_i\omega_i - jb_q}{\omega_i} \right) - \arctan\left(\dfrac{-\zeta_i\omega_i - ja_q}{\omega_i} \right) \right] \end{array} \right\}
\end{aligned} \tag{A12}$$

If damping is assumed negligible, $(b_q - a_q)/\omega_q \ll 1$, then Eq. (A12) reduces to

$$\mathrm{IME}_{kl}^{q} \approx \sum_{i=l}^{N} \left\{ \phi_k^i \phi_l^i (b_q - a_q) - \omega_i^2 \frac{\phi_k^i \phi_l^i j}{\omega_i} \left[\arctan\left(\frac{-\zeta_i \omega_i - j b_q}{\omega_i} \right) - \arctan\left(\frac{-\zeta_i \omega_i - j a_q}{\omega_i} \right) \right] \right\} \tag{A13}$$

When it is assumed that $\zeta_{i,j} = 0$ and $\zeta_i^2 \ll 1$, the derivative of the IME is

$$\mathrm{IME}_{kl,p}^{q} \approx \sum_{i=l}^{N} \left\{ \begin{array}{l} (b_q - a_q)\left(\phi_{k,p}^i \phi_l^i + \phi_k^i \phi_{l,p}^i\right) - j\omega_{i,p} \phi_k^i \phi_l^i \left[\arctan\left(\frac{-\zeta_i \omega_i - j b_q}{\omega_i} \right) - \arctan\left(\frac{-\zeta_i \omega_i - j a_q}{\omega_i} \right) \right] \\ -j\omega_i \left(\phi_{k,p}^i \phi_1^i + \phi_k^i \phi_{1,p}^i\right) \left[\arctan\left(\frac{-\zeta_i \omega_i - j b_q}{\omega_i} \right) - \arctan\left(\frac{-\zeta_i \omega_i - j a_q}{\omega_i} \right) \right] \\ -j\omega_i \phi_k^i \phi_l^i \left(\frac{j b_q \omega_{i,p}}{\omega_i^2 + 2\zeta_i \omega_i b_q j - b_q^2} - \frac{j a_q \omega_{i,p}}{\omega_i^2 + 2\zeta_i \omega_i a_q j - a_q^2} \right) \end{array} \right\} \tag{A14}$$

References

[1] Doebling, S. W., Farrar, C. R., Prime, M. B., and Shevitz, D. W., "Damage Identification and Health Monitoring of Structural and Mechanical Systems from Changes in Their Vibration Characteristics: A Literature Review," Los Alamos National Lab., TR LA-13070-MS, Albuquerque, NM, May 1996.

[2] Marwala, T., "Fault Identification Using Neural Networks and Vibration Data," Ph.D. Dissertation, Dept. of Engineering, Univ. of Cambridge, Cambridge, England, U.K., Aug. 2000.

[3] Kalos, M. H., and Whitlock, P. A., "Monte Carlo Methods," *Basics*, Wiley, New York, 1986, pp. 5–20.

[4] Ewins, D. J., "Modal Testing: Theory and Practice," *Engineering Dynamics Series*, 2nd ed., Research Studies, Letchworth, England, U.K., 1995.

[5] Fox, R. L., and Kapoor, M. P., "Rates of Change of Eigenvalues and Eigenvectors," *AIAA Journal*, Vol. 6, No. 1, 1968, pp. 2426–2429.

[6] Gradshteyn, I. S., and Yyzhik, I. M., "Tables of Integrals, Series, and Products," *Mathematics Tables*, Academic Press, London, 1994, pp. 81, 82.

[7] Balmès, E., "Structural Dynamics Toolbox User's Manual," Ver. 2.1, Scientific Software Group, Sèvres, France, 1997.

[8] "MATLAB Reference Guide," Mathworks, Natick, MA, 1992.

[9] Cooley, J. W., and Tukey, J. W., "An Algorithm for the Machine Calculation of Complex Fourier Series," *Mathematics of Computation*, Vol. 19, No. 1, 1965, pp. 297–301.

[10] Langley, R. S., "A Non-Poisson Model for Vibration Analysis of Uncertain Dynamic Systems," *Proceedings of the Royal Society of London, Series A: Mathematical, Physical and Engineering Sciences*, Vol. 455, No. 1, 1999, pp. 3325–3349.

[11] Friswell, M. I., and Mottershead, J. E., "Finite Element Model Updating in Structural Dynamics," *Solid Mechanics and Its Applications*, Kluwer Academic, Dordrecht, The Netherlands, 1995, p. 2.

A. Berman
Associate Editor